Microchimica Acta (2020) 187: 100
https://doi.org/10.1007/s00604-019-4073-6

ORIGINAL PAPER

A nickel–cobalt bimetallic phosphide nanocage as an efficient electrocatalyst for nonenzymatic sensing of glucose

Yanyan Zhu[1] · Yalin Wang[1] · Kai Kang[1] · Yulong Lin[1] · Wei Guo[1] · Jing Wang[1]

Received: 15 August 2019 / Accepted: 6 December 2019 / Published online: 7 January 2020

Abstract

The authors describe Ni–Co bimetal phosphide (NiCoP) nanocages that exhibit enhanced electrocatalytic performance toward glucose oxidation. The nanocages offer an appealing architecture, large specific area, and good accessibility for the analyte glucose. When placed on a glassy carbon electrode, the sensor exhibits attractive figures of merit for sensing glucose in 0.1 M NaOH solution including (a) a wide linear range (0.005–7 mM), (b) a low determination limit (0.36 μM), (c) high sensitivity (6115 $\mu A \cdot \mu M^{-1} \cdot cm^{-2}$), (d) a relatively low working potential (0.50 V vs. Ag/AgCl), and (e) good selectivity, reproducibility, and stability. The sensor is successfully applied to the determination of glucose in human serum samples.

Keywords Electrochemical sensor · Electrocatalytic activity · Hollow nanostructure · High sensitivity · Cyclic voltammetry · Good selectivity · Amperometric · Electron transport · Electrocatalytic oxidation · Human serum

Introduction

Electrochemical sensors are an attractive and practical technique for monitoring glucose levels in real-time and rapidly diagnosing diabetes [1, 2]. At present, conventional enzymatic electrochemical sensors based on glucose oxidase dominate the global market because of their high selectivity and sensitivity [3, 4]. Unfortunately, these sensors also suffer from several drawbacks, such as high cost, poor chemical and thermal stability, and complicated immobilization procedure of glucose oxidase [1, 2]. To address these issues, researchers have sought to develop non-enzymatic glucose sensors based on cost-effective and abundant-element inorganic nanomaterials [2]. The nanomaterial can directly catalyze glucose electrooxidation, including transition metal oxides [5–11], alloy [12, 13], hydroxides [14, 15], sulfides [16], nitride [17], phosphides [3, 4, 18–24], and carbon materials [5, 25]. Transition metal phosphides, such as Ni_2P, CoP, and Cu_3P, have been exploited in non-enzymatic glucose sensors due to their approximate zero-valent metallic feature, high electrocatalytic activity, and low cost [3, 4, 18, 20–24, 26]. For instance, Zhang et al. developed a Ni_2P nanoarray on conductive carbon cloth (Ni_2P NA/CC) as a glucose sensor with a low determination limit of 0.18 μM [4]. Wang et al. reported a MOF-derived porous Ni_2P/graphene composite with enhanced electrochemical properties in a glucose sensor and a low determination limit of 0.44 μM [19]. Das et al. developed Co_2P-encapsulated N/P dual doped carbon nanotubes with a determination limit of 0.88 μM [20]. Great progress has been achieved in the research of monometallic transition metal phosphides. Sun et al. found that bimetallic phosphides of NiCoP nanosheet arrays on a Ti mesh exhibit enhanced sensing performance compared with Ni_2P and CoP [22]. The combination of Ni and Co can enhance the electrocatalytic activity of phosphides in hydrogen or oxygen evolution reactions [27–29]. Hence, bimetal phosphides are hypothesized to be superior agents of glucose electrocatalysis in comparison with their monometallic counterparts.

The electrocatalytic activity of electrocatalysts toward glucose molecules affects the performance of the sensor, which is closely related to the structure of electrocatalysts [30–32].

Yanyan Zhu and Yalin Wang contributed equally to this work.

Electronic supplementary material The online version of this article (https://doi.org/10.1007/s00604-019-4073-6) contains supplementary material, which is available to authorized users.

✉ Yanyan Zhu
zhuyanyan@hebmu.edu.cn

✉ Jing Wang
jingwang@home.ipe.ac.cn

[1] School of Pharmaceutical Sciences, Hebei Medical University, Zhongshan East Road 361, Shijiazhuang 050017, People's Republic of China

Hollow nanostructure electrocatalysts have gained increased attention because of their large surface area, which allow more accessible catalytic sites with target molecules, produce a favorable catalytic interface, and facilitate electron/ion transport [27, 33]. With hollow nanostructures, the catalytic reaction kinetics is significantly promoted and the electrocatalytic activity of the catalysts toward glucose may be greatly improved.

Herein, we report the synthesis of Ni–Co bimetal phosphides nanocages (NiCoP) via a modified method [27] to obtain high-performance non-enzymatic electrochemical sensors. The resulting NiCoP nanocages show well-defined hollow porous structures and exhibit enhanced electrocatalytic activity toward glucose, outperforming Ni_2P or CoP nanocages alone.

Experimental section

Chemicals

NaOH (≥96.0%), KCl (≥99.5%), $K_3[Fe(CN)_6]$ (≥ 99.5%), $K_4[Fe(CN)_6]$ (≥ 99.5%), $Na_2S_2O_3$ (99%), lactose (Lac, 98%), absolute ethanol (≥ 99.5%) were purchased from Sinopharm Chemical Reagent Co., Ltd. (China, http://www.reagent.com.cn). $CuCl_2{\cdot}2H_2O$ (99.0%), $NiCl_2{\cdot}6H_2O$ (99.0%), $CoCl_2{\cdot}6H_2O$ (99.0%), NaH_2PO_2 (99.0%), D-(+)-glucose (≥ 99.5%), ascorbic acid (AA, >99%), uric acid (UA, ≥99%), dopamine (DA, ≥98%), fructose (Fru, 99%) were purchased from Aladdin Ltd. (Shanghai, China, http://www.aladdin-e.com/). Poly(vinyl pyrrolidone) was purchased from Alfa Aesar (Shanghai, China). Nafion (5 wt.%) was purchased from Sigma-Aldrich (St. Louis, MO, USA, http://www.Sigmaaldrich.com). All reagents were used without further purification. Human serum was obtained by Shijiazhuang First Hospital (Shijiazhuang, China).

Synthesis of the NiCoP nanocages

Synthesis of Cu_2O Cubes: Cu_2O cubes were synthesized according to a previously reported method [27]. Typically, 0.17 g of $CuCl_2{\cdot}2H_2O$ was added to 100 mL of double-distilled water and stirred for 30 min at 55 °C. Exactly 10 mL of 2 M NaOH was then slowly introduced to the mixture to form a brown suspension. Afterward, 10 mL of 0.6 M ascorbic acid was added to the system, which was aged for 3 h until the color of the suspension turned brick red. All steps were performed in a 55 °C water bath. The product was collected by centrifugation, washed several times with distilled water and ethanol, and then dried at 40 °C overnight under vacuum conditions.

Synthesis of $NiCo(OH)_2$ Nanocages: $NiCo(OH)_2$ nanocages were synthesized in the light of Pearson's HSAB principle [27]. In a typical procedure, 10 mg of Cu_2O was dispersed in 10 mL of a mixed solvent of double distilled water and absolute ethanol by ultrasonication for 30 min. Then, 0.33 g of poly(vinyl pyrrolidone) was added to the mixture, and ultrasonication was performed for another 30 min. Afterward, 3.4 mg of $NiCl_2{\cdot}6H_2O$ and $CoCl_2{\cdot}6H_2O$ (molar ratio of 1:1) were introduced to the above suspension. The solution was stirred for 30 min, followed by the slow injection of 20 mL of 1 M $Na_2S_2O_3$ until the color of the solution changed from brick red to transparent green, which suggests the formation of $NiCo(OH)_2$. The resulting precipitate was obtained by centrifugation, washed with distilled water and ethanol, and dried at 40 °C overnight under vacuum. For comparison, $Ni(OH)_2$ and $Co(OH)_2$ can be obtained by adding $NiCl_2{\cdot}6H_2O$ and $CoCl_2{\cdot}6H_2O$, respectively.

Synthesis of NiCoP Nanocages: The NiCoP nanocages were prepared according to a modified reported method [27]. In a typical reaction, 10 mg of $NiCo(OH)_2$ and 100 mg of NaH_2PO_2 were ground together for 10 min, placed in a quartz boat at the center of a tube furnace, and then heated at 300 °C for 2 h at a ramping rate of 5 °C min^{-1} in a N_2 atmosphere. Finally, the product was collected via washing with distilled and ethanol, and dried at 40 °C overnight under vacuum conditions. Ni_2P and CoP were prepared with $Ni(OH)_2$ and $Co(OH)_2$, respectively, via the same method.

Electrochemical measurements

Electrochemical tests were conducted on a CHI650E workstation with a three-electrode system; here, a glassy carbon electrode (GCE, 3 mm diameter), a Pt wire, and an Ag/AgCl electrode were used as the working, counter, and reference electrodes, respectively. The GCE was sequentially polished with 1.0, 0.5, and 0.05 μm alumina powder and then cleaned by ultrasound treatment with ethanol and ultrapure water. The working electrode was prepared as follows. Approximately 2 mg of the catalyst was dispersed in 500 μL of ethanol and 20 μL of Nafion (5 wt%) and then ultrasonicated to form a homogeneous suspension. Afterward, 5 μL of the suspension was dripped onto the GCE, which was then dried in air.

Characterization

The morphology of the sample was studied by field-emission scanning electron microscopy (JEM-7001F, https://www.jeol.co.jp/en/). TEM, HRTEM, high-angle annular dark-field scanning transmission electron microscopy (HAADF-STEM), and elemental mapping were conducted using a field-emission high-resolution transmission electron microscope (HRTEM, JEM-2010, https://www.jeol.co.jp/en/) equipped with EDX spectrometer. XRD patterns were obtained using an X-ray diffractometer (XRD, PANalytical Empyrean, http://www.panalytical.com) with Co Kα radiation (1.79 Å) operated at 40 kV and 100 mA. X-ray photoelectron spectroscopy (XPS)

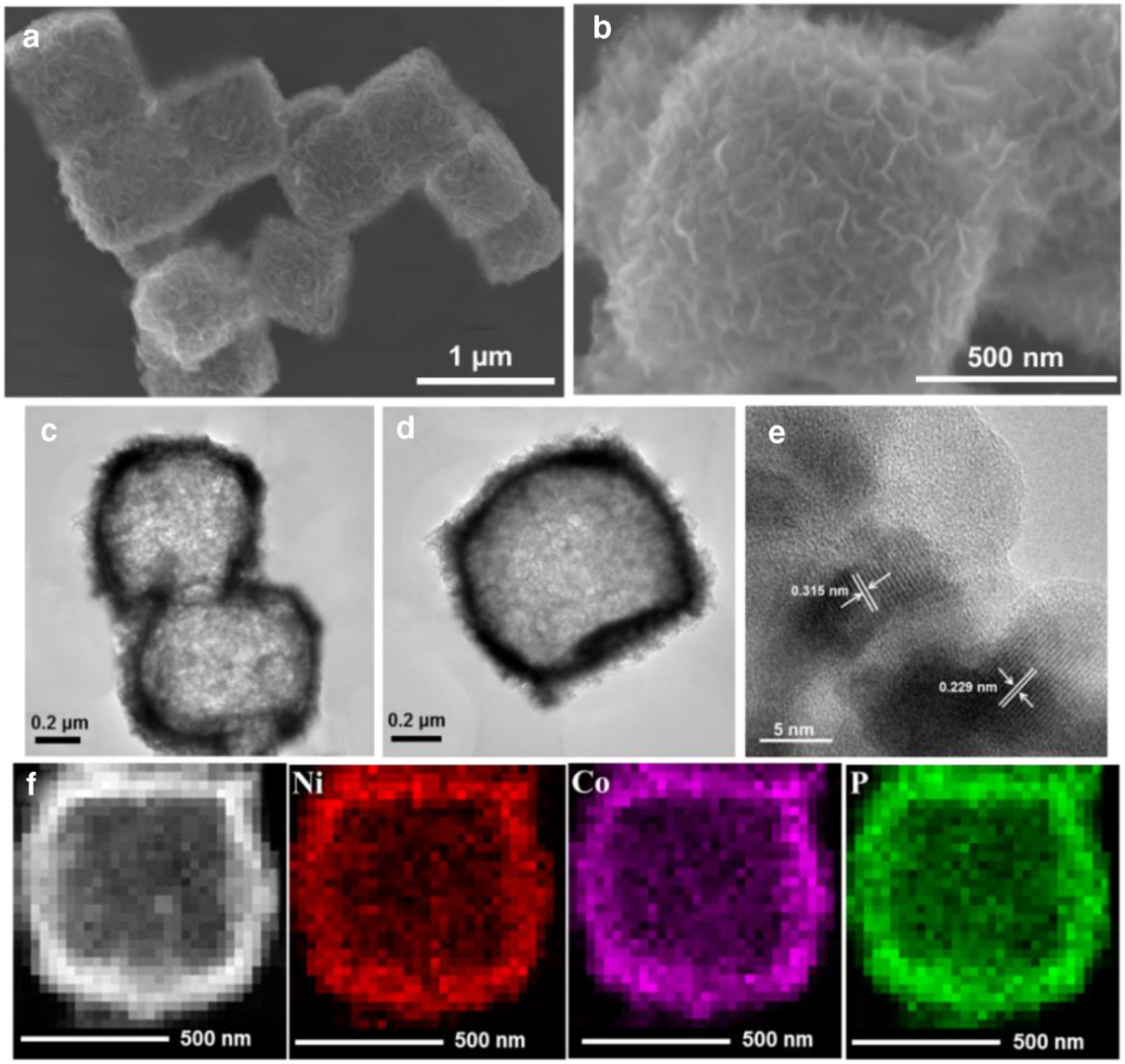

Fig. 1 NiCoP nanocages of SEM images (**a**) and (**b**), TEM images of (**c**) and (**d**), HRTEM image of (**e**), HAADF-STEM image of (**f**) and its corresponding element mapping images of Ni, Co, P

was conducted on an AXIS ULTRA DLD analyzer (https://www.kratos.com/).

Results and discussion

Characterization of NiCoP nanocages

To synthesize the NiCoP nanocages, Cu_2O nanocube templates are first synthesized through a wet-chemical method [27]. Typical SEM images (Figs. S1a and S1b) of the Cu_2O shows nanocube structures show smooth surfaces and a uniform diameter of 650 nm. The $NiCo(OH)_2$ nanocages are then prepared by adding equal molar ratios of Ni^{2+} and Co^{2+} in the presence of $Na_2S_2O_3$. SEM images of the $NiCo(OH)_2$ products display high-quality nanocages with an average size of 750 nm (Figs. S1c and S1d). Finally, the NiCoP products are obtained through a solid-state phosphorization of the $NiCo(OH)_2$ nanocages. The SEM images in Figs. 1a and b show that the NiCoP products maintain a structure identical to that of the $NiCo(OH)_2$ nanocages during phosphorization. For comparison, Ni_2P and CoP nanocages are also prepared using the method applied to obtain the NiCoP nanocages. SEM images of these nanocages (Figs. S2a and S2b) confirm that Ni_2P and CoP possess similar structures.

TEM and HRTEM are performed to probe the microstructure of the NiCoP nanocages. The TEM images of the NiCoP present a well-defined hollow and porous structure (Figs. 1c and d). Such a structure can offers a large active surface area and promotes the mass transport of electrocatalysts [27, 33]. The HRTEM image of the NiCoP nanocages in Fig. 1e shows two different well-resolved lattice fringes with lattice plane distances of approximately 0.229 and 0.315 nm,

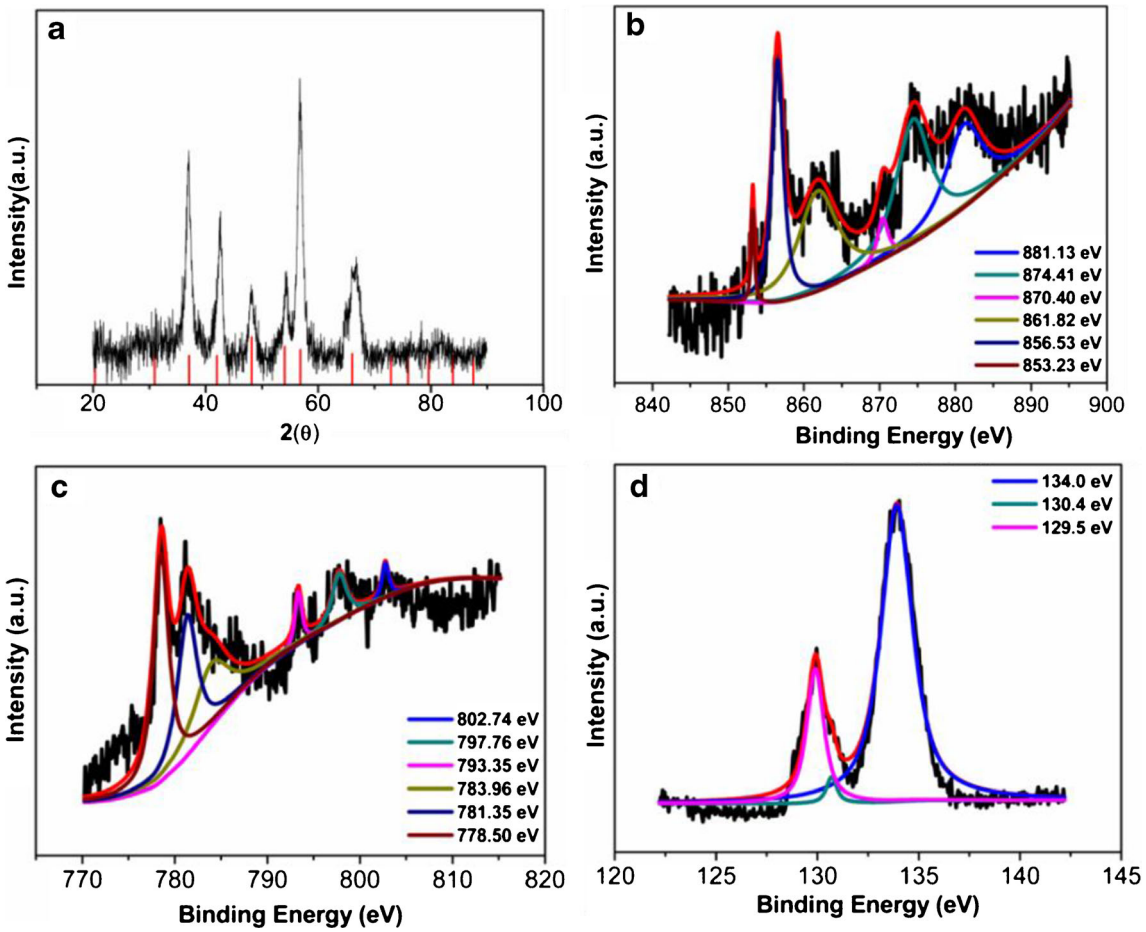

Fig. 2 **a** XRD pattern of NiCoP sample, high-resolution XPS spectra of NiCoP for **b** Ni 2p, **c** Co 2p, and P 2p

corresponding to the (201) and (110) planes of NiCoP, respectively. The spatial distribution of the different elements of one NiCoP nanocage is investigated by HAADF-STEM, and Ni, Co, and P are clearly homogeneously distributed throughout the NiCoP nanocage (Fig. 1f).

The crystal structure and composition of the NiCoP nanocages are investigated by using XRD. The XRD pattern (Fig. 2a) reveals the nanocage products matched well with the NiCoP phase (JCPDS 71–2261) [22, 27]. The surface chemical composition of NiCoP is elucidated by XPS, and the spectrum (Fig. S3) indicates the presence of Ni, Co, P, and O atoms in the NiCoP nanocage, which is consistent with previous reports [22]. The XPS spectrum of Ni $2p_{3/2}$ can be deconvolved into three peaks, among which the peaks at 856.53 eV and 853.23 are related to Ni^{3+} and Ni^{2+} species, respectively; a satellite peak occurring at 861.82 eV is also observed (Fig. 2b) [22, 27]. The binding energy of Ni in NiCoP (856.53 eV) is negatively shifted compared with that of Ni in Ni_2P (857.2 eV), thereby implying a strong electron interaction between Ni and Co atoms that causes charge redistribution [27]. In the Ni $2p_{1/2}$ spectrum, two obvious peaks located at 870.40 and 874.41 eV are respectively indexed to the Ni^{3+} and Ni^{2+} species in Ni-P and accompanied by a satellite peak (881.13 eV) [22, 27]. The high-resolution Co 2p spectrum in Fig. 2c reveals two peaks centered at 793.35 and 778.50 eV, which are respectively attributed to the Co $2p_1/2$ and Co $2p_{3/2}$ of Co species in Co-P. This finding suggests that the Co in NiCoP has a partial positive charge from the Co metal (777.9 eV). The two peaks at 797.76 and 781.35 eV are respectively related to the Co $2p_{1/2}$ and Co $2p_{3/2}$ of the oxidized Co species [27]. The main peaks at 802.74 and 783.96 eV can be matched to two shake-up satellites peak ("Sat."). The P 2p spectrum (Fig. 2d) exhibits two peaks at 130.4 and 129.5 eV. These can be assigned to P^{3-}. The main peak at 134.0 eV corresponds to PO_4^{3-} [27].

Electrochemical performance of NiCoP nanocages

The electrochemical performance of the NiCoP nanocages is investigated by CV in 0.1 M NaOH electrolyte with and without 2 mM glucose using a standard three-electrode system at a scan rate of 50 mVs^{-1} within the potential range of 0–0.8 V. The bare GCE is electrochemically inactive in the absence of glucose. NiCoP/GCE exhibits a pair of redox peaks at about 0.52 and 0.40 V. These can be assigned to the conversion of Ni(II)/Ni(III) and Co(II)/Co(III) (Fig. 3a) [4, 19, 20, 23].

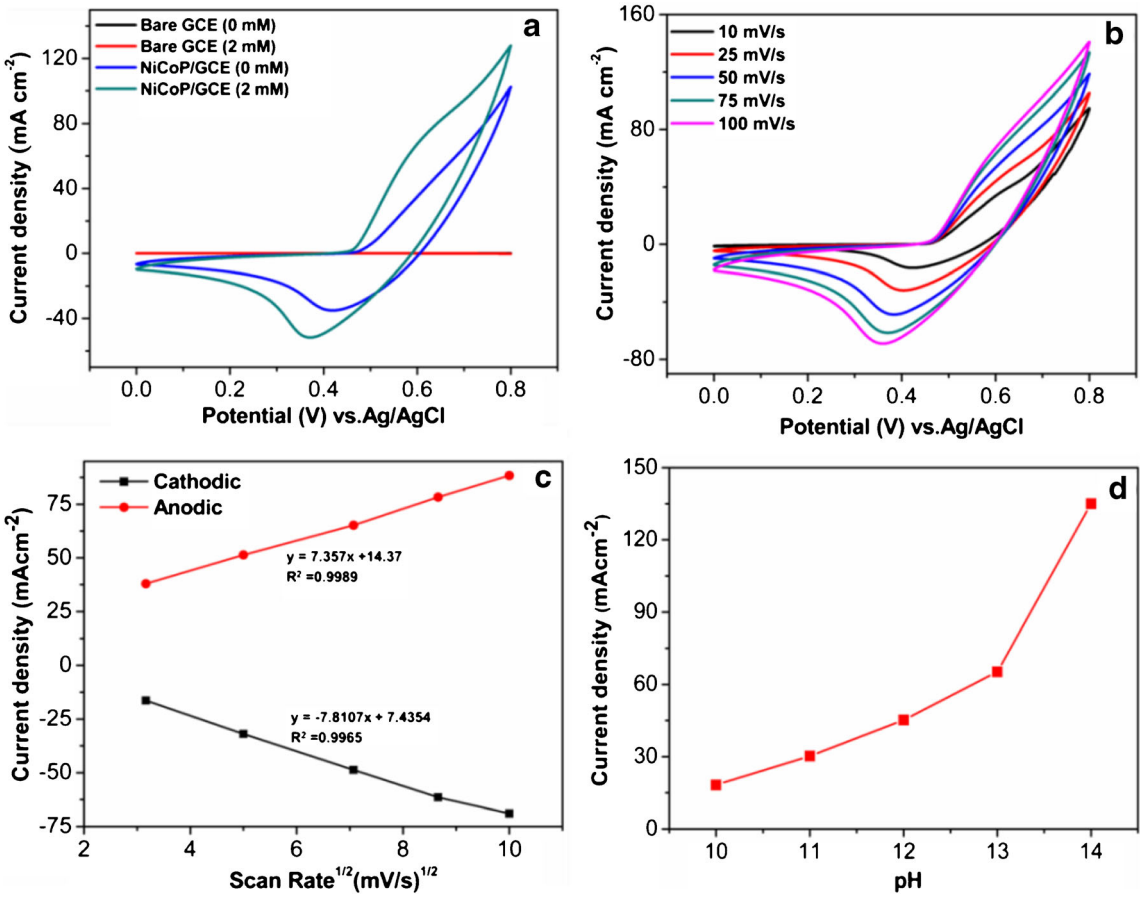

Fig. 3 **a** CV curves of bare GCE and NiCoP/GCE in 0.1 M NaOH in the absence and presence of 2 mM glucose at scan rate of 50 mV s^{-1}, **b** CV curves of NiCoP/GCE in 2 mM glucose at scan rates from 10 to 100 mV s^{-1}, **c** Corresponding plots of current density vs. the square root of scan rate, and **d** Plot of anodic peak current density vs pH for NiCoP/GCE in 2 mM glucose at scan rate of 50 mV s^{-1}

Given these results, concluding that a surface redox reaction occurs between $NiO_x/Ni(OH)_x$ and NiO(OH), as well as between $CoO_x/Co(OH)_x$ and CoO(OH), in the alkaline electrolyte is reasonable [4, 20]. The reaction can be formulated as:

$$NiO_x/Ni(OH)_x + OH^- - e^- \rightarrow NiOOH$$
$$CoO_x/Co(OH)_x + OH^- - e^- \rightarrow CoOOH$$

Upon injection of 2 mM glucose, NiCoP/GCE exhibits a notable increase in oxidation peak, whereas a negligible change occurs for the bare GCE; this result reveals the excellent catalytic activity of the former toward glucose oxidation. Enhancement of the oxidation current is attributed to the oxidation of glucose to gluconolactone with the participation of NiOOH and CoOOH accompanied by the conversion of Ni(III) to Ni(II) and Co(III) to Co(II). This conversion can be explained by the following formula:

$$Ni(III) + Co(III) + glucose \rightarrow Ni(II) + Co(II) + gluconolactone$$

Specifically, the NiCoP/GCE illustrates a higher anodic peak compared with those of Ni_2P and CoP GCEs (Fig. S4) in the presence and absence of glucose. This result suggests that the enhanced catalytic activity of NiCoP/GCE and the improved performance of NiCoP may arise from synergistic effects between Ni and Co to improve the electrochemical kinetics of glucose oxidation [22]. To gain insights into the electrochemical kinetics of NiCoP, EIS is utilized to probe the charge transfer properties of the modified electrodes at the electrode-electrolyte interface in 0.1 M KCl with 10 mM $K_3[Fe(CN)_6]$ and 10 mM $K_4[Fe(CN)_6]$, and the Nyquist plots are depicted in Fig. S5. The charge transfer resistance (R_{ct}) of NiCoP/GCE is significantly lower than those of Ni_2P/GCE and CoP/GCE, thereby implying maximum electrocatalytic activity of NiCoP/GCE [34]. The electrochemical effective areas of different modified electrodes are studied by chronocoulometry method in 0.1 mM $K_3[Fe(CN)_6]$ solution containing 1.0 M KCl (Fig. S6a) and can be obtained according to the Anson equation [35] $Q(t) = 2nFAcD^{1/2}\ t^{1/2}/\pi^{1/2} + Q_{dl} + Q_{ads}$, where n is the number of electron transfer ($n = 1$), F is Faraday constant, A is the effective area of electrode, c is the concentration of $K_3[Fe(CN)_6]$ (0.1 mM), D is the diffusion coefficient of $K_3[Fe(CN)_6]$ ($7.6 * 10^{-6}$ cm^2 s^{-1}), Q_{dl} and Q_{ads} are the double layer charge and Faradaic charge,

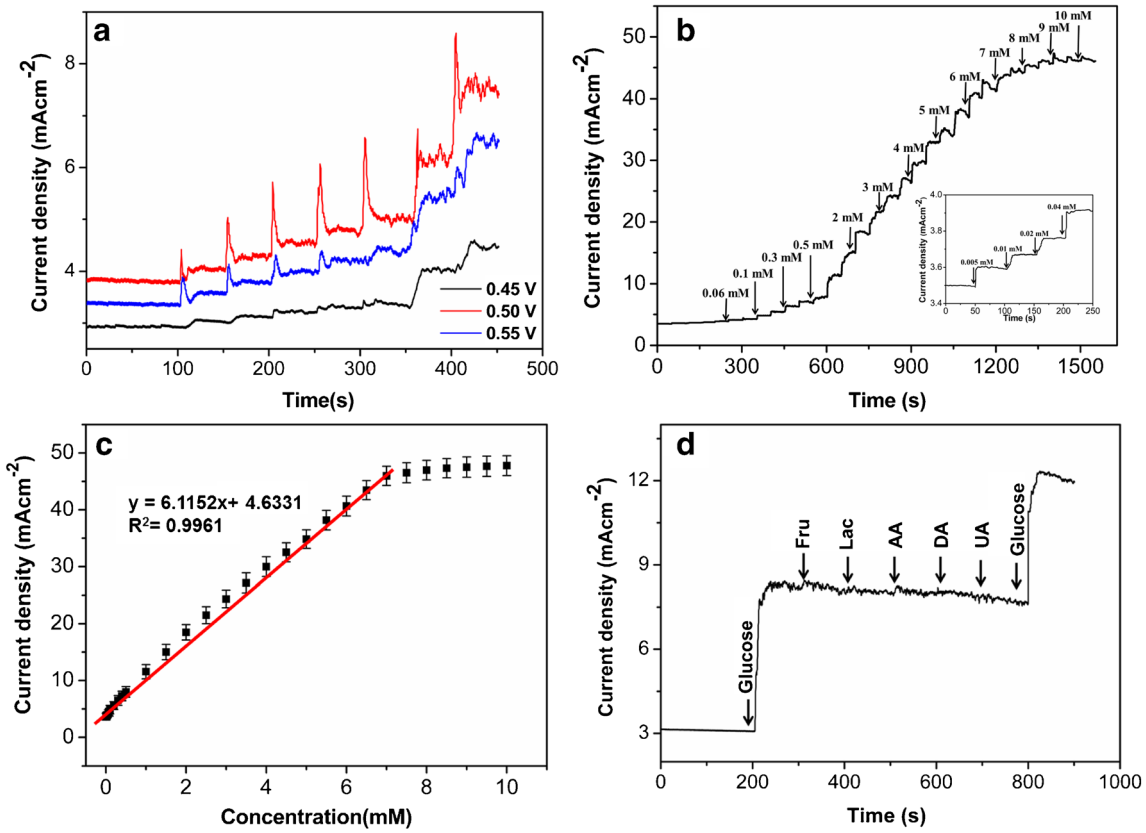

Fig. 4 **a** Amperometric responses of NiCoP/GCE at different potential in 0.1 M NaOH with addition of 20 μM, 40 μM, 60 μM, 80 μM, 100 μM, 200 μM, and 300 μM glucose, **b** amperometric response of NiCoP/GCE to glucose at 0.50 V, inset is the current response of NiCoP/GCE toward low concentrations of glucose, **c** the calibration plot for amperometric responses of NiCoP/GCE, **d** amperometric response of NiCoP/GCE toward addition of glucose and various interfering species in 0.1 M NaOH

respectively. The effective areas of NiCoP/GCE (0.126 cm^2), Ni_2P/GCE (0.089 cm^2), CoP/GCE (0.102 cm^2) and bare GCE (0.068 cm^2) are calculated from the slopes of the straight lines in Fig. S6b. Evidently, the result represents the larger effective area of NiCoP/GCE, implying the enhanced electrocatalytic activity of NiCoP/GCE. Encouraged by the excellent catalytic activity of NiCoP, the effect of scan rates in the sweep range of 10–100 mV s^{-1} on the glucose oxidation by NiCoP/GCE is

Table 1 Comparison of sensing performances of NiCoP nanocages with other reports on the non-enzymatic electrochemical glucose sensors

Electrode	Sensitivity (μA mM^{-1} cm^{-2})	Linear Range (mM)	Determination Limit (μM) (S/*N* = 3)	Reference
Cu_3P NW/CF	–	0.005–1	0.32	[3]
Ni_2P NA/CC	7792	0.001–3.0	0.18	[4]
CuO_x/NiO_y	2043	0.0002–2.5	0.08	[6]
NPG/$NiCo_2O_4$ needle	0.3871	0.01–21.24	1	[11]
PtNi alloy	40.17	0.5–40	0.35	[12]
Ni_3N NA	39	0.002–7.5	0.48	[17]
Ni_2P/G	7234	0.005–1.4	0.44	[19]
Co_2P/NPCNTs	338.8	~ 7	0.88	[20]
NiCoP/Ti	14,586	1–10	0.13	[22]
Pd–NiP	1136	0.5–10.24	0.15	[23]
Pd NPs/Ni-P	242.5 ± 3.28	0.002–4.65	0.91	[24]
CoP	116.8	~ 5.5	9	[26]
NiCoP Nanocage	6115	0.005–7	0.36	This work

Table 2 Determination of glucose in human serum samples of diabetic patients

Samples	Measured by glucometer (mM) Mean ± SD ($n = 3$)	Concentration determined by our sensor (mM) Mean ± SD ($n = 3$)	Recovery (%)	P
1	9.96 ± 0.05	9.65 ± 0.23	98.1	0.09
2	10.92 ± 0.03	10.53 ± 0.31	96.9	0.15
3	12.35 ± 0.02	12.02 ± 0.25	97.5	0.13

depicted in Fig. 3b. The peak currents linearly increase with the square root of the scan rates and have good correlation coefficient of 0.9989 and 0.9965 (Fig. 3c), which implies that glucose oxidation by NiCoP is regulated by a diffusion-controlled process [19, 30]. The influence of pH in the range of 10–14 on the electrochemical responses of NiCoP toward 2 mM glucose is also investigated. It can be seen in Fig. 3d that the anodic peak current linearly increases in the pH range of 10–13. A dramatic increase in anodic current occurs at pH 14, likely because of the oxygen evolution reaction [4, 19]. Hence, pH 13 is selected for further experiments.

Amperometric response curves are used to investigate the non-enzymatic glucose sensing performance of NiCoP. Fig. 4a displays the effect of applied potentials in the range of 0.45–0.55 V on the current response of the NiCoP/GCE with incremental additions of glucose to 0.1 M NaOH. The current response gradually increases with the rise of potential range from 0.45 to 0.5 V, but background currents and noise signals become apparent at 0.55 V. Thus, 0.5 V is adopted in subsequent experiments. The amperometric responses of NiCoP/GCE are recorded by the successive addition of glucose to 0.1 M NaOH at 0.5 V, and the amperometric response of the NiCoP/GCE toward glucose is displayed in Fig. 4b. The calibration plot (Fig. 4c) exhibits a linear relationship between the current response and the glucose concentration range from 0.005 to 7 mM with a correlation coefficient (R^2) of 0.9961. The NiCoP/GCE shows a high sensitivity of 6115 μA mM^{-1} cm^{-2} and a low determination limit of 0.36 μM (signal-to-noise ratio $S/N = 3$). The analytical performance of our glucose sensor compares favorably with those of other previously reported non-enzymatic electrochemical glucose sensors (Table 1).

The selectivity ability of the NiCoP/GCE is examined to evaluate the selectivity of this non-enzymatic sensor. The amperometric responses of the NiCoP/GCE with continuous injection of 1 mM glucose, 0.2 mM fructose (Fru), 0.2 mM lactose (Lac), 0.2 mM ascorbic acid (AA), 0.2 mM dopamine (DA), 0.2 mM uric acid (UA), and 1 mM glucose in 0.1 M NaOH at 0.50 V are illustrated in Fig. 4d. An obvious and fast increase in the current response can be observed with the addition of glucose. By contrast, the increase in current is negligible after the addition of AA, UA, DA, Fru, and Lac [3, 4, 32]. In the reproducibility test, six different NiCoP/GCEs prototypes were investigated with 1 mM glucose in 0.1 M NaOH and the relative standard deviation is only 3.61%, thereby implying the good reproducibility of this sensor. The stability of the NiCoP/GCE is tested by monitoring the current response of 1 mM glucose for 1 month and the NiCoP/GCE is stored at room temperature with exposure to air; only a slight attenuation of 3.72% of the original current is observed (Fig. S7); this result suggests the excellent stability of the NiCoP/GCE based sensor.

The potential application of the NiCoP/GCE to clinical practice is evaluated by detecting glucose in human serum samples from diabetics. The concentration of each serum sample is determined via the amperometric response curve by the addition of the serum sample (100 μL) to 0.1 M NaOH (10 mL) under stirring at 0.50 V. The concentrations (Table 2) determined by this sensor are consistent with those by a commercial glucometer. The P values (Table 2) determined by the t-test were all higher than 0.05 between the proposed sensor and glucometer, implying the there was no obvious difference between the proposed sensor and glucometer. The results suggest that NiCoP/GCE has potential applications in non-enzymatic electrochemical sensors for detecting glucose in real human serum samples.

Conclusions

NiCoP nanocages are demonstrated to be highly active electrocatalysts toward glucose oxidation under alkaline conditions on account of their structural and compositional advantages. The NiCoP nanocages display enhanced electrocatalytic activity for glucose compared with Ni_2P and CoP. As a non-enzymatic glucose sensor, the NiCoP nanocage electrode shows excellent performance, such as a low determination limit, high sensitivity, and good selectivity, reproducibility, and stability. This study provides new perspectives in the design of efficient catalyst electrode materials for high-performance sensing applications.

Acknowledgments The authors gratefully acknowledge the financial support from the Natural Science Foundation of Hebei Province (Grant No. B2019206437, H2017206214), Chunyu Project Outstanding Youth Fund of Hebei Medical University (No. CYYQ201903), the Undergraduate Innovation Project (No. USIP2019092), and the Education Department of Hebei Province of China for Funding

Through the Innovative Hundred Talents Support Program (SLRC2017047).

Compliance with ethical standards

The author(s) declare that they have no competing interests.

Ethics statement The human serum was used in this manuscript with the informed consent of the donors. The experimental design and protocols used in this study were approved by the Regulation of the Hebei Medical University of Research Ethics Committee.

References

1. Hwang D-W, Lee S, Seo M, Chung TD (2018) Recent advances in electrochemical non-enzymatic glucose sensors – a review. Anal Chim Acta 1033:1–34
2. Dhara K, Mahapatra DR (2017) Electrochemical nonenzymatic sensing of glucose using advanced nanomaterials. Microchim Acta 185(1):49
3. Xie L, Asiri AM, Sun X (2017) Monolithically integrated copper phosphide nanowire: an efficient electrocatalyst for sensitive and selective nonenzymatic glucose detection. Sensor Actuat B-Chem 244:11–16
4. Chen T, Liu D, Lu W, Wang K, Du G, Asiri AM, Sun X (2016) Three-dimensional Ni_2P Nanoarray: an efficient catalyst electrode for sensitive and selective nonenzymatic glucose sensing with high specificity. Anal Chem 88(16):7885–7889
5. Vilian ATE, Dinesh B, Rethinasabapathy M, Hwang S-K, Jin C-S, Huh YS, Han Y-K (2018) Hexagonal Co_3O_4 anchored reduced graphene oxide sheets for high-performance supercapacitors and non-enzymatic glucose sensing. J Mater Chem A 6(29):14367–14379
6. Long L, Liu X, Chen L, Li D, Jia J (2019) A hollow CuO_x/NiO_y nanocomposite for amperometric and non-enzymatic sensing of glucose and hydrogen peroxide. Microchim Acta 186(2):74
7. Liu L, Wang Z, Yang J, Liu G, Li J, Guo L, Chen S, Guo Q (2018) $NiCo_2O_4$ nanoneedle-decorated electrospun carbon nanofiber nanohybrids for sensitive non-enzymatic glucose sensors. Sensor Actuat B-Chem 258:920–928
8. Li R, Liu X, Wang H, Wu Y, Chan KC, Lu Z (2019) Sandwich nanoporous framework decorated with vertical CuO nanowire arrays for electrochemical glucose sensing. Electrochim Acta 299:470–478
9. Huang Y, Tan Y, Feng C, Wang S, Wu H, Zhang G (2018) Synthesis of CuO/g-C_3N_4 composites, and their application to voltammetric sensing of glucose and dopamine. Microchim Acta 186(1):10
10. Foroughi F, Rahsepar M, Hadianfard MJ, Kim H (2017) Microwave-assisted synthesis of graphene modified CuO nanoparticles for voltammetric enzyme-free sensing of glucose at biological pH values. Microchim Acta 185(1):57
11. Li W, Qi H, Wang B, Wang Q, Wei S, Zhang X, Wang Y, Zhang L, Cui X (2018) Ultrathin $NiCo_2O_4$ nanowalls supported on a 3D nanoporous gold coated needle for non-enzymatic amperometric sensing of glucose. Microchim Acta 185(2):124
12. Wang R, Liang X, Liu H, Cui L, Zhang X, Liu C (2018) Non-enzymatic electrochemical glucose sensor based on monodispersed stone-like PtNi alloy nanoparticles. Microchim Acta 185(7):339
13. Lu L, Kang J (2018) Amperometric nonenzymatic sensing of glucose at very low working potential by using a nanoporous PdAuNi ternary alloy. Microchim Acta 185(2):111
14. Pal N, Banerjee S, Bhaumik A (2018) A facile route for the syntheses of $Ni(OH)_2$ and NiO nanostructures as potential candidates for non-enzymatic glucose sensor. J Colloid Interface Sci 516:121–127
15. Wang F, Zhang Y, Liang W, Chen L, Li Y, He X (2018) Non-enzymatic glucose sensor with high sensitivity based on cu-Al layered double hydroxides. Sensor Actuat B-Chem 273:41–47
16. Meng A, Yuan X, Li Z, Zhao K, Sheng L, Li Q (2019) Direct growth of 3D porous $(Ni\text{-}co)_3S_4$ nanosheets arrays on rGO-PEDOT hybrid film for high performance non-enzymatic glucose sensing. Sensor Actuat B-Chem 291:9–16
17. Luo J, Zhao D, Yang M, Qu F (2018) Porous Ni_3N nanosheet array as a catalyst for nonenzymatic amperometric determination of glucose. Microchim Acta 185(4):229
18. Liu Y, Cao X, Kong R, Du G, Asiri AM, Lu Q, Sun X (2017) Cobalt phosphide nanowire array as an effective electrocatalyst for non-enzymatic glucose sensing. J Mater Chem B 5(10):1901–1904
19. Zhang Y, Xu J, Xia J, Zhang F, Wang Z (2018) MOF-derived porous Ni_2P/Graphene composites with enhanced electrochemical properties for sensitive nonenzymatic glucose sensing. ACS Appl Mater Interfaces 10(45):39151–39160
20. Das D, Das A, Reghunath M, Nanda KK (2017) Phosphine-free avenue to Co_2P nanoparticle encapsulated N,P co-doped CNTs: a novel non-enzymatic glucose sensor and an efficient electrocatalyst for oxygen evolution reaction. Green Chem 19(5):1327–1335
21. Sedighi A, Montazer M, Mazinani S (2019) Synthesis of wearable and flexible $NiP_{0.1}$-SnO_x/PANI/CuO/cotton towards a non-enzymatic glucose sensor. Biosens Bioelectron 135:192–199
22. Wang Z, Cao X, Liu D, Hao S, Du G, Asiri AM, Sun X (2016) Ternary NiCoP nanosheet array on a Ti mesh: a high-performance electrochemical sensor for glucose detection. Chem Commun 52(100):14438–14441
23. Ma J, Chen Y, Chen L, Wang L (2017) Ternary Pd–Ni–P nanoparticle-based nonenzymatic glucose sensor with greatly enhanced sensitivity achieved through active-site engineering. Nano Res 10(8):2712–2720
24. Wang M, Ma Z, Li J, Zhang Z, Tang B, Wang X (2018) Well-dispersed palladium nanoparticles on nickel- phosphorus nanosheets as efficient three-dimensional platform for superior catalytic glucose electro-oxidation and non-enzymatic sensing. J Colloid Interface Sci 511:355–364
25. Amin BG, Masud J, Nath M (2019) A non-enzymatic glucose sensor based on a $CoNi_2Se_4$/rGO nanocomposite with ultrahigh sensitivity at low working potential. J Mater Chem A 7(14):2338–2348
26. Sun Q-Q, Wang M, Bao S-J, Wang YC, Gu S (2016) Analysis of cobalt phosphide (CoP) nanorods designed for non-enzyme glucose detection. Analyst 141(1):256–260
27. Qiu B, Cai L, Wang Y, Lin Z, Zuo Y, Wang M, Chai Y (2018) Fabrication of nickel–cobalt bimetal phosphide nanocages for enhanced oxygen evolution catalysis. Adv Funct Mater 28:1706008
28. He P, Yu X-Y, Lou XW (2017) Carbon-incorporated nickel–cobalt mixed metal phosphide Nanoboxes with enhanced Electrocatalytic activity for oxygen evolution. Angew Chem Int Ed 56(14):3897–3900
29. Tian J, Chen J, Liu J, Tian Q, Chen P (2018) Graphene quantum dot engineered nickel-cobalt phosphide as highly efficient bifunctional catalyst for overall water splitting. Nano Energy 48:284–291
30. Yang M, Jeong J-M, Lee KG, Kim DH, Lee SJ, Choi BG (2017) Hierarchical porous microspheres of the Co_3O_4@graphene with enhanced electrocatalytic performance for electrochemical biosensors. Biosens Bioelectron 89:612–619
31. Qazzazie D, Yurchenko O, Urban S, Kieninger J, Urban G (2017) Platinum nanowires anchored on graphene-supported platinum nanoparticles as a highly active electrocatalyst towards glucose oxidation for fuel cell applications. Nanoscale 9(19):6436–6447
32. Zhu Y, Zhang X, Sun J, Li M, Lin Y, Kang K, Meng Y, Feng Z, Wang J (2019) A non-enzymatic amperometric glucose sensor

based on the use of graphene frameworks-promoted ultrafine platinum nanoparticles. Microchim Acta 186(8):538
33. Guan BY, Yu L, Lou XW (2017) Formation of single-holed cobalt/N-doped carbon hollow particles with enhanced Electrocatalytic activity toward oxygen reduction reaction in alkaline media. Adv Sci 4(10):1700247
34. Mazaheri M, Aashuri H, Simchi A (2017) Three-dimensional hybrid graphene/nickel electrodes on zinc oxide nanorod arrays as non-enzymatic glucose biosensors. Sensor Actuat B-Chem 251: 462–471
35. Tian Q, Xu J, Zuo Y, Li Y, Zhang J, Zhou Y, Duan X, Lu L, Jia H, Xu Q, Yu Y (2019) Three-dimensional PEDOT composite based electrochemical sensor for sensitive detection of chlorophenol. J Electroanal Chem 837:1–9